1.5-kW, 150,000-r/min Ultra High-Speed PM Motor Fed by 12-V Power Supply for Automotive Supercharger

Toshihiko Noguchi*, and Tetsuro Wada**

* Shizuoka University
3-5-1 Johoku, Naka-Ku, Hamamatsu 432-8561, Japan
Tel.: +81-53-478-1128
Fax: +81-53-478-1128
E-Mail: ttnogut@ipc.shizuoka.ac.jp
** Nagaoka University of Technology
1603-1 Kamitomioka, Nagaoka 940-2188, Japan
Tel.: +81-258-47-6000
Fax: +81-258-47-9500
E-Mail: twada@stn.nagaokaut.ac.jp

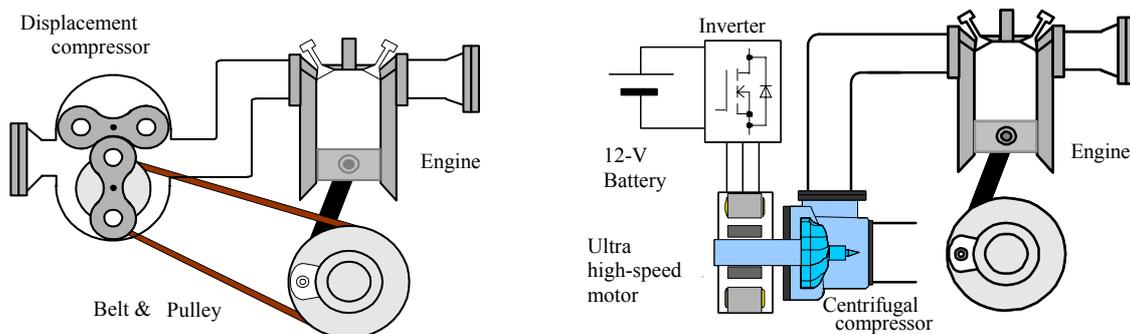## Acknowledgements

Keywords

«high speed drive», «permanent magnet motor», «adjustable speed drive», «automotive application», «automotive component».

Abstract

This paper presents a 1.5-kW, 150,000-r/min PM motor fed by a 12-V power supply, which is applicable to an automotive supercharger. The motor is specially designed to improve its efficiency over 97 % (excluding a mechanical loss) and to raise its power density to 13 W/cm^3 at the same time. Feasibility of the design is confirmed through experimental tests, using a prototype motor.

Introduction

A supercharger is an auxiliary machine to enhance output power of a combustion engine and to reduce the engine displacement at the same time. Employing the supercharger is also effective to improve the combustion efficiency, the exhaust gas quality and the engine torque response. The conventional supercharger has a mechanical linkage with the engine that uses a timing belt, and it compresses inlet air into the engine cylinders by means of the mechanical power provided by the engine. Figure 1 (a)

(a) Conventional system. (b) Electrically operated system.
Fig. 1: System configurations of conventional and electrically operated supercharging systems.

illustrates a mechanical configuration of the conventional supercharging system. As shown in the figure, many of the superchargers employ a positive displacement compressor because its operation speed is limited by a low revolution speed of the engine. However, the positive displacement compressor has drawbacks such as lower efficiency and lower boost pressure than those of a centrifugal compressor, which prevents further performance improvement of the supercharging system. In order to solve these problems, electrification of the supercharger is significantly important and is very promising approach as a next-generation auxiliary machine system for future automobiles. Figure 1 (b) shows an outline of the electrically operated supercharging system where an ultra high-speed permanent magnet (PM) motor is used to drive the centrifugal compressor instead of the conventional positive displacement compressor. Since the electrically operated supercharger allows use of the centrifugal compressor and makes a mechanical-linkage-free system possible, many advantages are obtained, e.g., more efficient operation, higher rotation speed, higher boost pressure, faster response of the inlet air compression, and smaller mechanical dimensions than those of the conventional displacement compressor based system. Furthermore, such a mechanical-linkage-free design gives freedom of mechanical placement around the engine, and makes it possible to reduce overall mechanical losses as well as to eliminate the complicated linkage mechanism.

This paper discusses an optimum design of the ultra high-speed PM motor of which specific application is the electrically operated supercharger of the automotive engine. The motor is fed by a three-phase inverter with a 12-V battery as a DC power supply for an automotive application; thus the motor design must meet a high-current and high-frequency operation requirement without sacrificing the motor efficiency and power density. The investigated motor has a rated output power of 1.5 kW and the maximum rotation speed of 150,000 r/min, respectively. In order to achieve this goal, various technical issues must be solved, e.g., drastic reduction of the synchronous impedance, minimization of the iron and the copper losses, further improvement of the motor efficiency and the power density, mechanical stabilization in high-speed operation range, and so forth. In addition, these electrical design requirements must be satisfied all together with a compact and robust mechanical design. On the way of optimization process in the machine design, a finite element method (FEM) based electromagnetic field analysis is conducted to make fine-tuning of the detailed motor shape and to maximize the efficiency and the power density at the same time. Consequently, the efficiency has been improved over 97 % (excluding a mechanical loss) and the power density has been raised to approximately 13 W/cm^3 in the prototype motor design.

Required Specifications of Ultra High-Speed PM Motor

Assuming a 1,500-cc class automotive engine, the ultra high-speed PM motor is required to have the rated power of 1.5 kW at the maximum rotation speed of 150,000 r/min to achieve the electrically operated supercharging system. When boosting the inlet air compression, extremely fast response is required because the compressor must be accelerated from several ten thousand r/min to the maximum rotation speed in approximately 0.5 s, which surpasses a response time of the conventional supercharger. In order to meet this requirement, the motor must have a short-duration overload capacity, which is a double of the rated output power for 1 s. Table I shows target specifications of the motor determined by the above requirement.

Basic Design Concept of Ultra High-Speed PM Motor

In order to achieve the highest efficiency and the highest power density among various sorts of electric motors, a two-pole three-phase surface permanent-magnet synchronous motor (SPMSM) is focused on

Table I: Specifications of developed ultra high-speed PM motor

Assumed engine	1500 cc class
Rated output power	1.5 kW
Maximum rotation speed	150,000 r/min
Rated torque	0.0955 Nm
Overload capacity and duration	3 kW (200 % load) for 1 s

as the best choice for the ultra high-speed motor drive because of the simple rotor structure and no magnetizing current required, which implies higher efficiency than other motors.

The stator has a six-tooth six-slot structure and concentrated windings, which is remarkably effective to reduce the copper loss and the leakage inductance thoroughly as well as the synchronous inductance. Each phase has a pair of single or double-turned windings in parallel, and the windings are not ordinary wires but copper bars of which shape is like an alphabetical letter "b." It is necessary to reduce as much stator iron loss as possible even at 150,000 r/min operation, so high-performance 6.5-% silicon electromagnetic steel plates of which thickness is only 0.1 mm are employed to compose a laminated stator iron core.

On the other hand, the rotor consists of a strong Nd-Fe-B permanent magnet and a molybdenum alloy shaft. Use of the Nd-Fe-B permanent magnet allows not only motor efficiency improvement but also drastic reduction of the rotor size and inertia. In addition, such a strong Nd-Fe-B permanent magnet that has $BH_{max} = 310$-kJ/m^3 makes it possible to widen the air gap, which is essential to reduce the synchronous inductance and to obtain a sinusoidal electromotive force (e.m.f.) regardless of the concentrated stator winding structure.

Table II is a summary of the basic conceptual design parameters of the ultra high-speed PM motor to be investigated in this paper.

Optimization of Permeance Coefficient and Stator Windings

Since a permeance coefficient determines an operating point on a B-H curve of the permanent magnet, operation characteristics of the PM motor dominantly depend on the permeance coefficient. The permeance coefficient is basically proportional to the e.m.f. unless other physical dimensions of the investigated motor are changed. Therefore, the permeance coefficient has a strong influence on the motor efficiency because there is a trade-off relationship between the copper loss and the iron loss of the motor, depending on the e.m.f. Assuming that the investigated PM motor has a uniform permeance distribution along the air gap, the permeance coefficient p_u of the motor is expressed by the following equation:

$$p_u = \frac{\ell_m}{a_m} \frac{a_g}{K_C \ell_g} = \frac{\ell_m}{D_m - \ell_m} \frac{D_m + \ell_g}{K_C \ell_g} \,, \tag{1}$$

where ℓ_m is a permanent-magnet thickness, a_m is an averaged cross section area of the permanent magnet, a_g is an averaged cross section area of the air gap between the rotor and the stator, ℓ_g is a radial air gap length, D_m is an outer diameter of the permanent magnet, and K_C is a Carter's coefficient. Since K_C normally takes a value of approximately 1.2 to 1.5, a_g can be regarded as almost same as $a_m K_C$; thus, the following approximated expression is obtained:

$$p_u \approx \frac{\ell_m}{\ell_g} \,. \tag{2}$$

This equation shows that the permeance coefficient is determined by the ratio between the permanent-magnet thickness and the radial air gap length as illustrated in Fig. 2.

Table II: Conceptual design parameters of developed ultra high-speed PM motor

Motor type	Surface Permanent-Magnet Synchronous Motor (SPMSM)
Number of phases	3 phase
Number of poles	2 pole
Stator winding configuration	Concentrated
Winding configuration	1- or 2-turn windings in parallel per phase
Electromagnetic steel plates	10JNEX900 (0.1-mm thick, 6.5-% silicon, μ_s = 23,000, B_{max} = 1.8 T)
Permanent magnet	Nd-Fe-B N-39SH (Br = 1.28 T, bHc = 955 kA/m, BH_{max} = 310 kJ/m^3)
Bearings	Angular ceramic-ball bearings with grease lubrication

The synchronous impedance of the investigated PM motor must ultimately be reduced because the motor is operated under high-current and high-frequency operation conditions. Otherwise, it is impossible to satisfy the target specifications, delivering the rated power of 1.5 kW at the maximum rotation speed of 150,000 r/min with a 12-V DC power supply. This ultimately low synchronous impedance can be accomplished by having a wide air gap owing to such a strong Nd-Fe-B permanent magnet as $BH_{max} = 310$ kJ/m^3, and by reducing the number of winding turns drastically. Figure 3 (a) indicates a stator winding configuration, where two models of the winding structure are illustrated in the same figure, i.e., a one-turn and a two-turn structures. The copper-bar windings are cut out of bulk copper plates so that their shape is like an alphabetical letter "b" as illustrated in Fig. 3 (b). The leakage inductance can effectively be reduced by inserting these windings closely to teeth of the stator iron core.

In general, a back e.m.f. of the PM motor is expressed as follows:

$$e = \sqrt{2}\,E = \sqrt{2}\,p\omega k_w N\phi_g \,, \tag{3}$$

where p is the number of pole pairs, ω is an operation speed in rad/s, k_w is a winding coefficient, N is the number of winding turns and ϕ_g is an air gap magnetic flux. As the above equation indicates, the back e.m.f. can be enlarged by increasing N or ϕ_g. Therefore, the two configurations of the stator windings shown in Fig. 3 (a) are investigated from the viewpoint of the efficiency and power density maximization and the voltage utilization of the inverter output. Suppose that each motor line current is controlled to be in phase with the back e.m.f. of the corresponding phase, the total phase voltage including a voltage drop of the inverter can be expressed by the following equation:

$$V = R_{FET}I + R_a I + \mathrm{j}\omega L_a I + E \,, \tag{4}$$

where $R_{FET}I$ is a voltage drop of the MOSFETs used in the inverter (approximately 2 mΩ/phase), $R_a I$ is a voltage drop of the stator winding resistance, $\omega L_a I$ is a voltage drop of the stator winding inductance, and E is the back e.m.f. The voltage drops of the motor with one-turn stator windings are listed in the left column of Table III. As can be seen in the table, the voltage drop due to the synchronous inductance is hardly observed as well as the leakage inductance drop. In addition, the back e.m.f. is
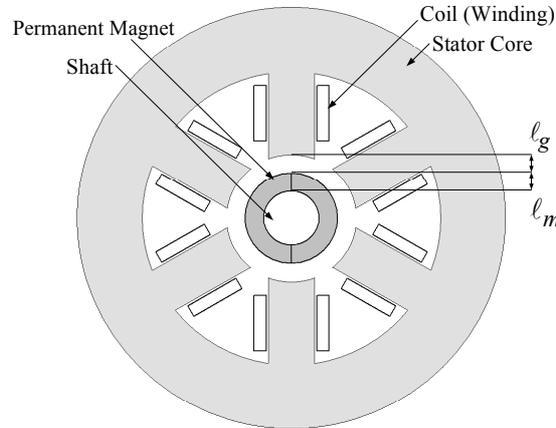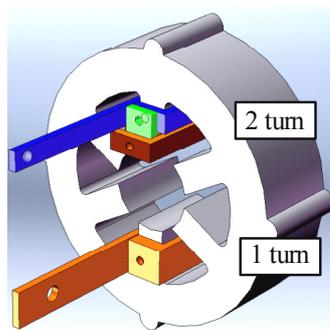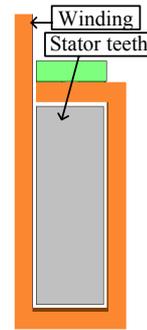

Fig. 2: Cross section diagram to investigate permeance coefficient.

(a) Stator core and windings.　　　　(b) Stator winding.

Fig. 3: Stator winding configuration.

unnecessarily too low to utilize the DC power supply voltage. Therefore, since both of the leakage inductance and the synchronous inductance are sufficiently small, it is possible to operate the motor with a 12-V DC power source even if the number of turn is double as indicated in the upper part of Fig. 3 (a), resulting in quadruple synchronous inductance and twice in the back e.m.f. In addition, changing the permeance coefficient p_u from 1.67 to 0.882 to improve the motor efficiency, the voltage drops of the motor with the two-turn stator windings are as listed in the right column of Table III. As described previously, the winding resistance and the inductance become 4 times of those in the one-turn motor, but the increase of these voltage drops can be restricted within 2.5 times to 2.9 times because the operating current is effectively reduced by approximately 30 % by optimizing the back e.m.f. Assuming that the maximum phase voltage applied to the motor is 4.9 V_{rms}, which can be fed by the inverter with the 12-V DC power supply, it is possible to utilize 90.0 % of the 12-V power supply voltage at 1.5-kW operation and to utilize 97.5 % even in a 200-% over load condition without a voltage saturation.

Optimization of Detailed Dimensions for Power Density Maximization

In order to maximize the power density of the motor without sacrificing the efficiency, the detailed stator iron core shape, i.e., a yoke width, a outer diameter and a tooth width, is investigated through FEM based electromagnetic analyses as shown in Fig. 4. The stator inner diameter is fixed at 28 mm, which is derived from the calculation result of the permeance coefficient described above and the stack length of the stator iron core is limited to 30 mm to prevent harmful mechanical vibrations of the
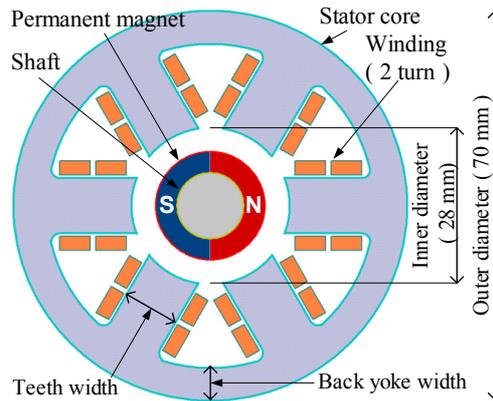

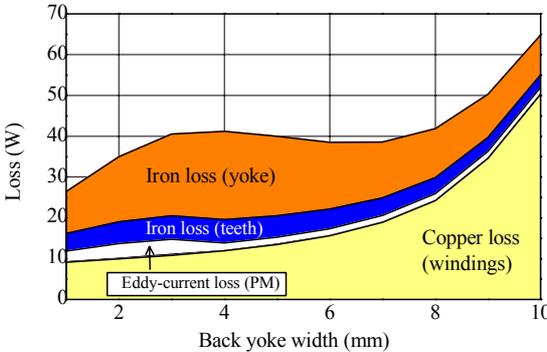Fig. 4: Cross section diagram of 2-turn PM motor.

Table III: Voltage drops per phase at rated operation and other design parameters

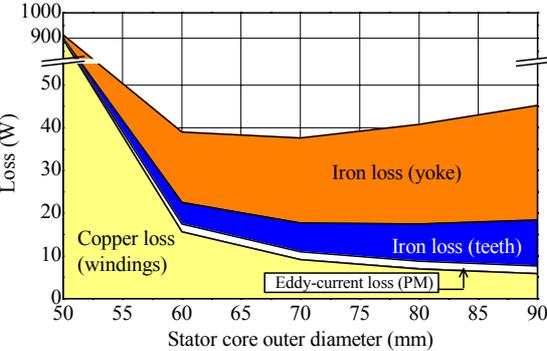| Number of winding turns	1	2
Resistance of inverter MOSFET R_{FET}	2 mΩ	
Stator winding resistance R_a	0.072 mΩ	0.200 mΩ
Stator winding inductance L_a	0.070 μH	0.294 μH
Voltage drop of inverter MOSFET $R_{FET}I$	0.353 V	0.243 V
Voltage drop of the stator winding resistance R_aI	0.0127 V	0.0243 V
Voltage drop of the stator winding inductance ωL_aI	0.194 V	0.562 V
Back e.m.f. E	2.84 V	4.11 V
Total voltage drop V	3.21 V	4.41 V
Stator iron core stack length L	30 mm	
Permanent-magnet thickness ℓ_m	5 mm	3.75 mm
Radial air gap length ℓ_g	3 mm	4.25 mm
Permeance coefficient p_u	1.67	0.882

rotor shaft over the whole operation speed range. Figure 5 shows loss analysis results of the motor with respect to the specified dimension of the stator iron core.

Figure 5 (a) shows electrical losses of the motor when only the stator yoke width is changed while other parameters, i.e., the stator outer diameter and the tooth width, are kept constant. As the stator yoke gets wider, the iron loss gradually decreases because the magnetic flux density is reduced in the iron core, but the copper loss becomes dominant among the losses. Since the copper loss is affected by the slot cross section area for the windings, the wider stator yoke reduces the slot cross section area, resulting in higher current density and higher resistance of the windings. On the other hand, when the stator yoke is too narrow, the motor is unable to deliver the torque due to the magnetic saturation in the stator yoke. Therefore, it can be found that 6 mm is the best value for the stator yoke width.
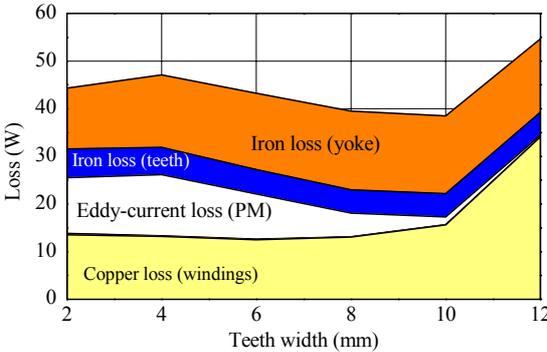
Keeping the stator yoke width at 6 mm, a loss analysis result is shown in Fig. 5 (b) as the stator outer diameter is changed. The reduction of the stator outer diameter makes the total iron core loss less because the magnetic flux path gets shorter together with whole volume of the motor. However, the percentage of the copper loss becomes more remarkable as the stator outer diameter gets smaller. The reason of this copper loss enlargement is excessive reduction of the slot cross section area for the windings. Therefore, the stator outer diameter of 70 mm takes the minimum loss, which is the most effective to optimize the overall motor dimensions from the viewpoint of the efficiency and the power density.

(a) Loss analysis result with respect to back yoke width.

(b) Loss analysis result with respect to stator outer diameter.

(c) Loss analysis result with respect to teeth width.
Fig. 5: Loss analysis results with respect to detailed stator iron core shape.

In a similar way, the tooth width can be determined to be 10 mm to minimize the total loss. As the tooth width gets narrower, it is found that the eddy current loss on the rotor permanent magnet becomes higher. This is because the wider slot opening due to the narrower tooth causes more detrimental permeance variation along the air gap.

Consequently, the detailed stator iron core and rotor dimensions are summarized as listed in Table IV. Since the total volume of the stator and the rotor including the air gap is only 115.5 cm^3, the power density at the rated output power reaches 13W/cm^3, which is approximately 10 times of that of common electric machines. The outer diameter of the rotor is as small as 19.5 mm; thus, the circumference velocity of the rotor reaches 153.2 m/s, which is less than half of the sound speed. As described later on, however, the rotor is mechanically reinforced by glass fiber threads with epoxy resin to prevent the permanent magnet rotor from destruction due to large centrifugal force.

Figure 6 shows loss comparison at the rated operating condition between the one-turn and the two-turn motors designed in this investigation. As can be seen in the figure, the two-turn motor achieves drastic reduction of the electrical losses down to 36 W, compared with those of the one-turn motor, i.e., 62 W. The copper loss of the two-turn motor is enlarged because of the small slot cross section area, but each of the eddy current loss on the rotor permanent magnet and the stator iron core loss is effectively reduced. It is inferred that the total efficiency of the designed two-turn motor excluding a mechanical loss reaches 97.6 % although the motor is driven by such a low-voltage DC power supply as a 12-V battery.

Prototype Ultra High-Speed PM Motor

As described in the basic design concept, the prototype has a special electrical and mechanical structure. Figure 7 shows photographs of the prototype. The laminated stator iron core consists of approximately 300 sheets of 6.5-% silicon electromagnetic steel plates, of which outer diameter is 70 mm, inner diameter is 28 mm, and axial stack length is 30 mm. The stator winding copper bars are inserted in the stator teeth with keeping electrical insulation from the stator iron core by polyimide taping, and are connected to a neutral-point end ring all together. Each of the stator windings has a cross section area of 16 mm^2, resulting in a current density of 7.6 A/mm^2 at the rated operating condition. Every clearance between each tooth and each stator winding is less than 0.3 mm, which effectively improves the magnetic coupling with reducing the leakage flux.

On the other hand, the rotor is simply assembled with a ring-shaped Nd-Fe-B permanent magnet and a molybdenum alloy shaft, and is magnetized so that the flux distribution becomes sinusoidal. After assembling the rotor, 2.5-mm thick layer of the non-electrically-conductive glass fiber is formed with special epoxy resin on the permanent magnet surface against large centrifugal force. Mechanical reinforcement with glass fiber can be seen in the photograph of the rotor exterior.

Table IV: Summary of designed dimensions

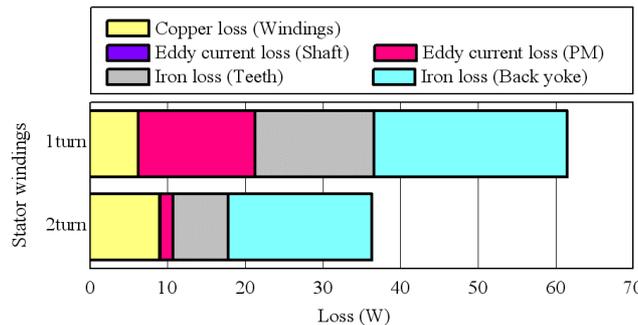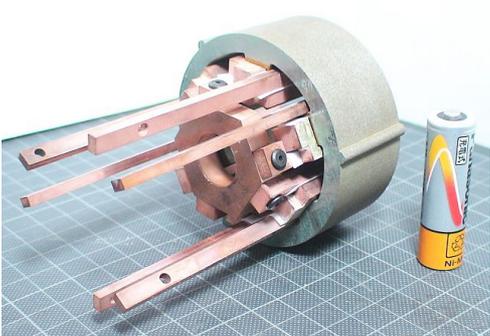|			
Stator outer diameter *DO*	70 mm	Stator stack length *L*	30 mm
Stator inner diameter *DI*	28 mm	Rotor PM outer diameter *dO*	19.5 mm
Stator yoke width *YW*	6 mm	Rotor PM thickness ℓ_m	3.75 mm
Stator tooth width *TW*	10 mm	Radial air gap length ℓ_g	4.25 mm

Fig. 6: Loss comparison between one-turn and two-turn motors at rated operating condition.

Figure 8 illustrates a three-dimensional computer graphic (a bird's-eye view) of the prototype motor assembly. All of the metal components are made with a high-precision NC machining tools. The prototype is designed and created to have extremely high mechanical accuracy of μm-order, especially in the bearing brackets and the rotor shaft parts.

Experimental Setup and Test Results

Figure 9 shows a schematic diagram of an experimental setup to confirm basic operation characteristics of the prototype motor. A pseudo current-source inverter was employed to drive the motor because of a high-fundamental-frequency over 2 kHz and extremely low-synchronous inductance. The pseudo current-source inverter consists of a current-controlled buck-boost chopper and a six-step inverter. The former is operated with a DC-bus current feedback at a switching frequency of 48 kHz, resulting in significant reduction of the DC-bus reactor inductance. The latter commutates the DC-bus current and generates 120-deg conduction patterns of the motor line currents. Surge voltages during the current commutation are clamped by the DC-bus power source via MOSFETs' body diodes and a bypass diode in the chopper.

Table V represents comparison between the designed and the measured motor parameters. As listed here, the measured motor inductance is slightly higher than the designed value because of the leakage inductance and the line inductance to the motor.

(a) Stator iron core with two-turn windings.

(b) Nd-Fe-B PM rotor reinforced by glass fiber.

(c) Front and rear views of assembled motor.

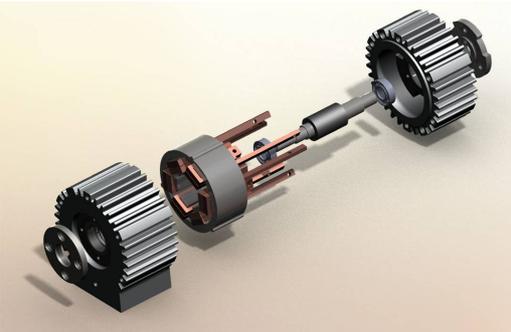Fig. 7: Photographs of prototype ultra high-speed PM motor.

Fig. 8: Three-dimensional computer graphic of motor assembly.

Figure 10 shows steady-state waveforms of the Hall-effect position sensor signal, the line current and the terminal voltage of the motor operated at 150,000 r/min under no load condition. As can be seen in the figure, the 120-deg current pattern is properly generated in synchronism with the Hall-effect position sensor signal. The motor terminal voltage is sinusoidal without a conspicuous harmonic distortion, which implies the back e.m.f. is properly generated so as to be a sinusoidal waveform by the rotor permanent magnet regardless of the concentrated winding structure of the stator.

Figure 11 shows an acceleration test result, which was conducted to examine the output torque controllability. Since measuring the mechanical output at such an ultra high-speed as 150,000 r/min is rather difficult, the output torque of the prototype motor was estimated by a designed value of the rotor inertia and an acceleration observed in the speed step response. As shown in the figure, it is inferred that the maximum output torque delivered for the acceleration was approximately 0.08 Nm due to the current limit of the inverter, which was 84 % of the rated value. Although the estimated output torque waveform is choppy, it can be found from the waveform envelope that the speed is linearly regulated.

Conclusion

This paper discussed an optimum design to develop a 1.5-kW, 150,000-r/min ultra high-speed PM motor fed by a 12-V DC power source, which is applicable to an automotive supercharger, from the viewpoint of efficiency and power density improvement. The prototype has various unique features in its electrical and mechanical structure, which achieves a low-voltage, high-current and high-frequency operation. Owing to the optimum design of the permeance coefficient and the detailed stator iron core shape, the designed motor can achieve an ultimately high power density of 13 W/cm^3 together with a remarkably high efficiency over 97 % (excluding a mechanical loss). The maximum-speed operation under no-load condition and a speed step response with a 84-% output torque delivered were experimentally examined, and proper operation characteristics were confirmed through the experimental tests.
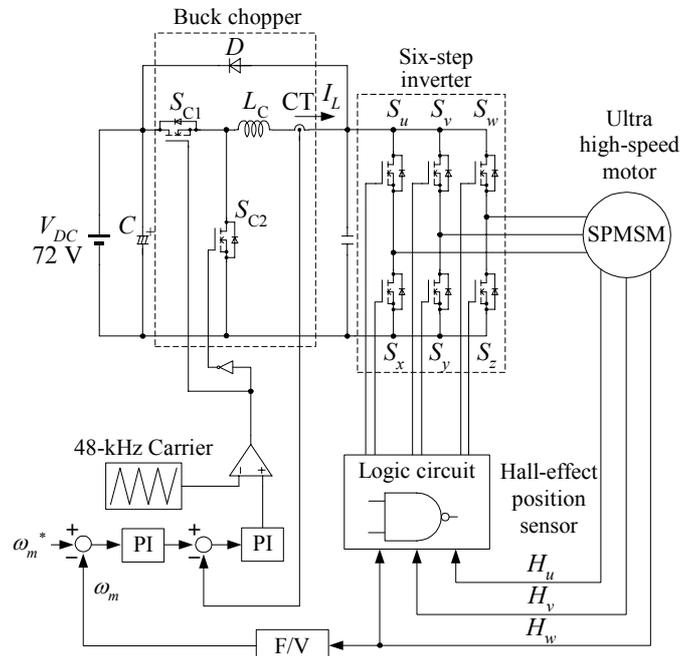

Fig. 9: Schematic diagram of pseudo current-source inverter drive.

Table V: Measurement result of two-turn motor parameters

Motor parameters	Designed value	Measured value
E.m.f constant	2.74 x 10^{-5} V/r/min	2.67 x 10^{-5} V/r/min
Stator winding resistance R_a	0.200 mΩ	0.151 mΩ
Stator winding inductance L_a	0.294 μH	0.362 μH

References

[1] M. Okawa, "Design Manual of Magnetic Circuit and PM Motor," *Sogo Research*, 1989 (in Japanese).

[2] I. Takahashi, T. Koganezawa, T. Su G., and K. Ohyama, "A Super High Speed PM Motor Drive System by a Quasi-Current Source Inverter," *IEEE Transactions on Industry Applications*, Vol. 30, no. 3, p.p. 683-690, 1994.

[3] B. -H. Bae, and S. -K. Sul, "A Compensation Method for Time Delay of Full-Digital Synchronous Frame Current Regulator of PWM AC Drives," *IEEE Transactions on Industry Applications*, Vol. 39, no. 3, p.p. 802-810, 2003.

[4] B. -H. Bae, S. -K. Sul, J. -H. Kwon, and J. -S. Byeon, "Implementation of Sensorless Vector Control for Super-High-Speed PMSM of Turbo-Compressor," *IEEE Transactions on Industry Applications*, Vol. 39, no. 3, p.p. 811-818, 2003.

[5] T. Noguchi, Y. Takata, Y. Yamashita, Y. Komatsu, and S. Ibaraki, "220000r/min, 2-kW Permanent Magnet Motor Drive for Turbocharger", *IEE-Japan International Power Electronics Conference (IPEC2005) -Niigata*, p.p. 2280-2285, 2005.

[6] C. Zwyssig, M. Duerr, D. Hassler, and J. W. Kolar, "An Ultra-High-Speed, 500000 rpm, 1 kW Electrical Drive System," *The Fourth Power Conversion Conference (PCC2007) -Nagoya*, CDROM, 2007.

[7] T. Noguchi, and M. Kano, "Development of 150000 r/min, 1.5 kW Permanent-Magnet Motor for Automotive Supercharger," *The Seventh International Conference on Power Electronics and Drive Systems (PEDS2007) -Bangkok*, 2A-03, 2007.
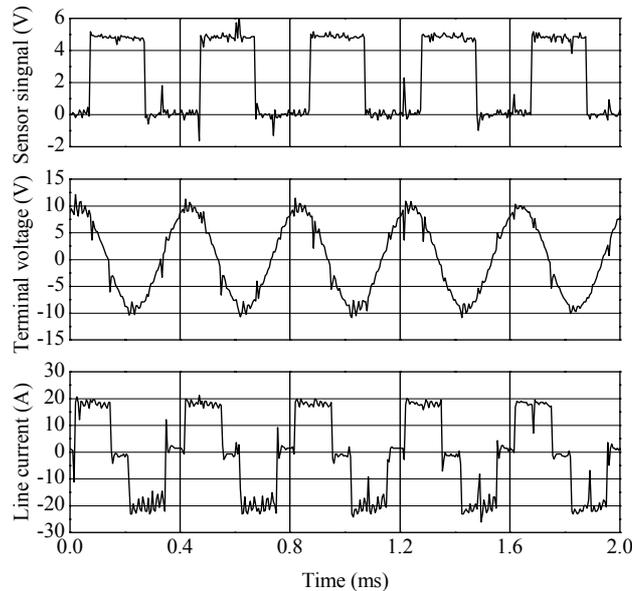
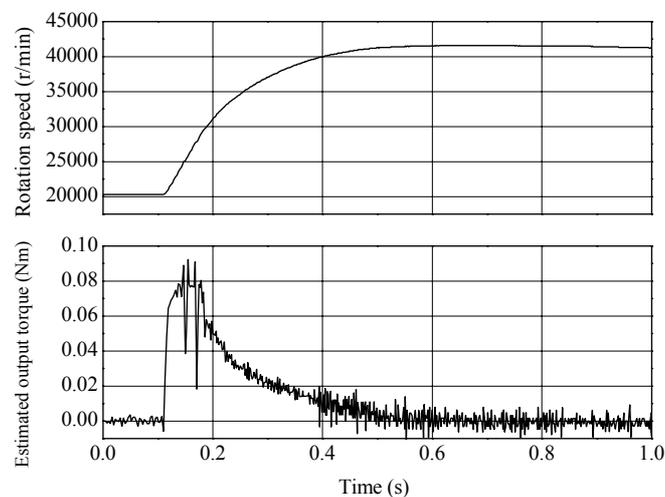Fig. 10: Operating waveforms at 150,000 r/min under no load condition.

Fig. 11: Speed step response and experimentally estimated output torque.